添付図　1

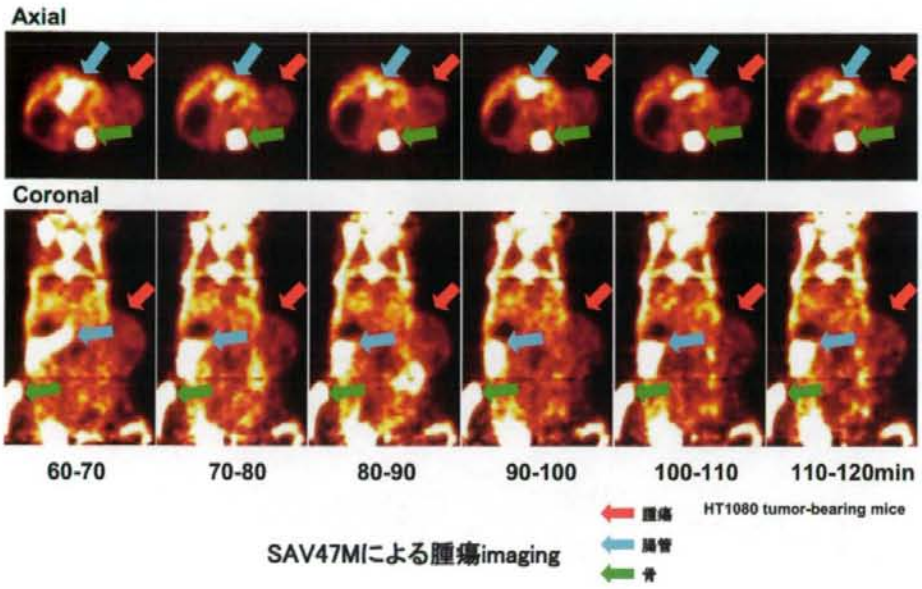

SAV47Mによる腫瘍imaging

添付図　2　(SAV49の合成)

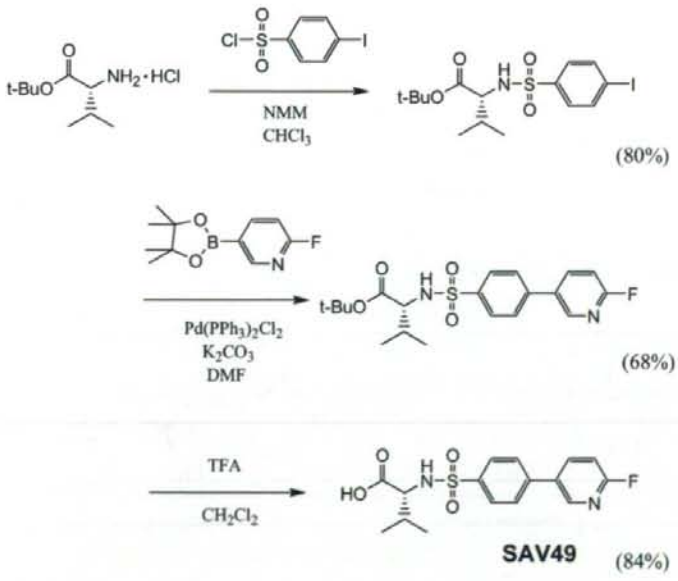

添付図　3　([^{18}F]SAV49M標識前駆体合成)

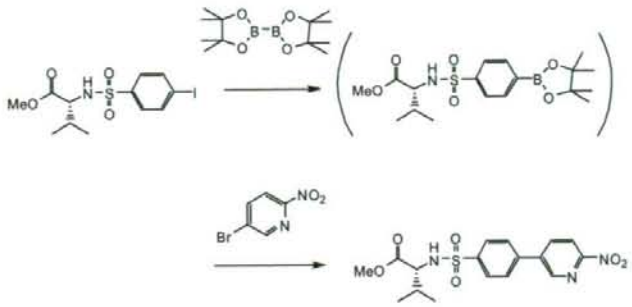

[^{18}F]SAV49M標識前駆体

添付図　4　([^{18}F]SAV49M標識反応)

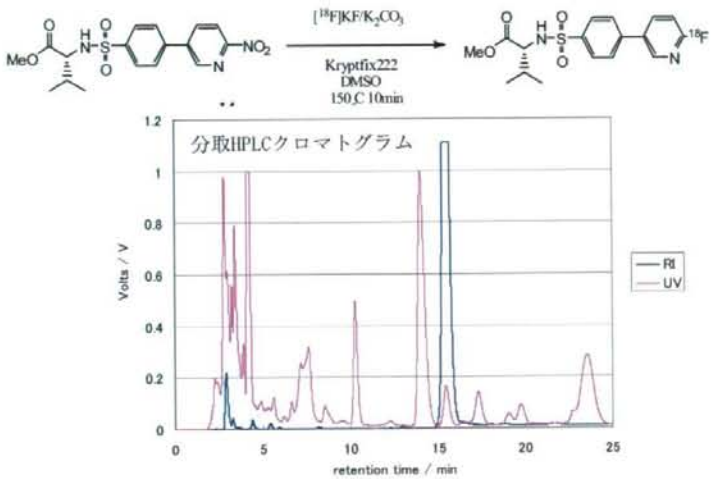

添付図　5　([^{18}F]FMISOのR体とS体の構造式)

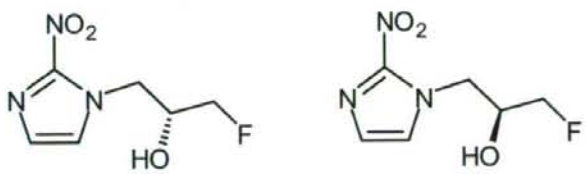

(R)-[^{18}F]FMISO　　(S)-[^{18}F]FMISO

厚生労働科学研究費補助金（医療機器開発推進研究事業）
分担研究報告書

高磁場ＭＲＩと核医学・分子イメージングに基づく動脈硬化の高感度かつ定量的な診断と新しい予防戦略の構築

分担研究者　佐藤博司　国立循環器病センター研究所
先進医工学センター　先進診断機器開発室

研究要旨

不安定プラークの進展過程において特徴的な構造的・質的変化を可視化する高磁場MRI撮像技術を開発することを目的とする。磁場強度3Tにおいてプラーク検出に必要なコイル群、シーケンス群を整備し、そのパラメータを最適化した。

A．研究目的

不安定プラークの進展過程において特徴的な構造的・質的変化を可視化する高磁場MRI撮像技術を開発する。

B．研究方法

磁場強度3T MRI装置 GE Healthcare社製SIGNA HDを使用し、これまでに開発してきた食道部Phased Arrayコイルを頚動脈、頭蓋内MCA領域のプラーク検出に応用する。シーケンスは微小プラークをターゲットとするため高分解能化を目指し、かつ臨床的な撮像時間を越えない条件で最適化を行う。ボランティアにおいて基本的な最適化を行い、最終的にプラークの疑われる患者において評価を行う。基本的な縦緩和時間強調像、横緩和時間強調像の両方を撮像しコントラストを比較する。

C．研究結果

1回の撮像が概ね15分を超えると動きによるアーチファクトが大きくなる傾向があり、特に患者においては画像が著しく悪化することがあり、撮像をやり直さなければならなくなることが多くなった。そこでT1,T1とも10分前後の撮像時間で、最小限の信号強度比を保ちつつ、空間分解能をあげるように最適化を行った。コイルはボールジョイントによる可動式の構造で、被検体の様々な頸部形状に合わせて、固定することが可能であった。頸部においてはソレノイドタイプと８の字タイプのコイルの２つをフェーズドアレイ化し、それを左右２つ配置して、計4チャンネルのフェーズドアレイ駆動が信号強度比の観点から有効であった。図１はボランティアにおける同一部位（頸動脈分岐部）における縦緩和時間強調像、横緩和時間強調像、アンギオグラフィ、プロトン密度強調画像を示す。頸動脈部は心拍に同期した動きによるぼけが、高分解能化を制限するため、指先の赤外線センサーによる脈拍に撮像を同期させた（縦緩和時間強調像、横緩和時間強調像）。また血管周辺における脂肪組織の信号が血管内部のプラークの信号と紛らわしくなるため反転回復法による脂肪組織信号の減弱化を行った。図２に拡大像を示す。血管内部がその周辺組織との関係を含め十分な分解能で撮像可能であることが確認できた。またマルチコントラストによる多角的な評価が行えるため質的評価に言及可能と思われる。

さらにプラークの置かれた分子環境的な情報を得るため、磁化移動法による画像化を試みた。磁化移動法ありとなしの画像の比から磁化移動比を算出し、緩和時間強調像、横和時間強調像と比較したものを図３に示す（MCA BAD患者）。縦緩和時間強調像、横緩和時間強調像とはまったく異なる新しいコントラストが得られており、今後病態との関係を評価していくことが期待された。

高分解能画像のマルチスライス化を行い、1コントラストあたり約10分という制約のなかで、十分な領域を対象とすることが可能であることを確認した（図４）。

得られた結果を患者において評価した（図５）。脳底部動脈における血腫、血栓、解離を描出することが可能であることを確認した。また頭蓋内中大脳動脈においてはPerforator起始部における梗塞がBAD患者の患側において観察することができた（図６）。

マルチ
コントラスト
による
多角的評価

T1w Double IR FR-FSE 2D PG-Gated HR85Bpm, Delay711ms, TR1412s, TE10, SpSati, FatSat, ETL 12, Bw122Hz/pix, Res0.254^2x2mm, Res0.254^2x2mm, NEX4, Scan Time2min

MRA SPGR-3D FA20, TR42ms, TE5ms, SpSats, FC, MT, Bw122Hz/pix, Res0.254^2x2mm, NEX1, Scan Time 10min

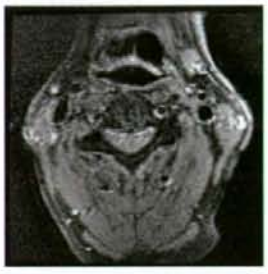

T2w Double IR FR-FSE 2D PG-Gated HR85Bpm, Delay711ms, TR1412ms, TE76, SpSati, FatSat, ETL 24, Bw81Hz/pix, Res0.254^2x2mm, NEX8, Scan Time2min

PD FSE 2D TR5s, TE12, SpSati, FatSat, ETL 12, Bw122Hz/pix, Res0.254^2x2mm, Res0.254^2x2mm, NEX2, Scan Time10min

図1　頚動脈部マルチコントラストによる多角的評価

拡大像

T1w Double IR FR-FSE 2D PG-Gated HR85Bpm, Delay711ms, TR1412s, TE10, SpSati, FatSat, ETL 12, Bw122Hz/pix, Res0.254^2x2mm, Res0.254^2x2mm, NEX4, Scan Time2min

MRA SPGR-3D FA20, TR42ms, TE5ms, SpSats, FC, MT, Bw122Hz/pix, Res0.254^2x2mm, NEX1, Scan Time10min

T2w Double IR FR-FSE 2D PG-Gated HR85Bpm, Delay711ms, TR1412ms, TE76, SpSati, FatSat, ETL 24, Bw81Hz/pix, Res0.254^2x2mm, NEX8, Scan Time2min

PD FSE 2D TR5s, TE12, SpSati, FatSat, ETL 12, Bw122Hz/pix, Res0.254^2x2mm, Res0.254^2x2mm, NEX2, Scan Time10min

図2　頚動脈部マルチコントラスト頚動脈部拡大像

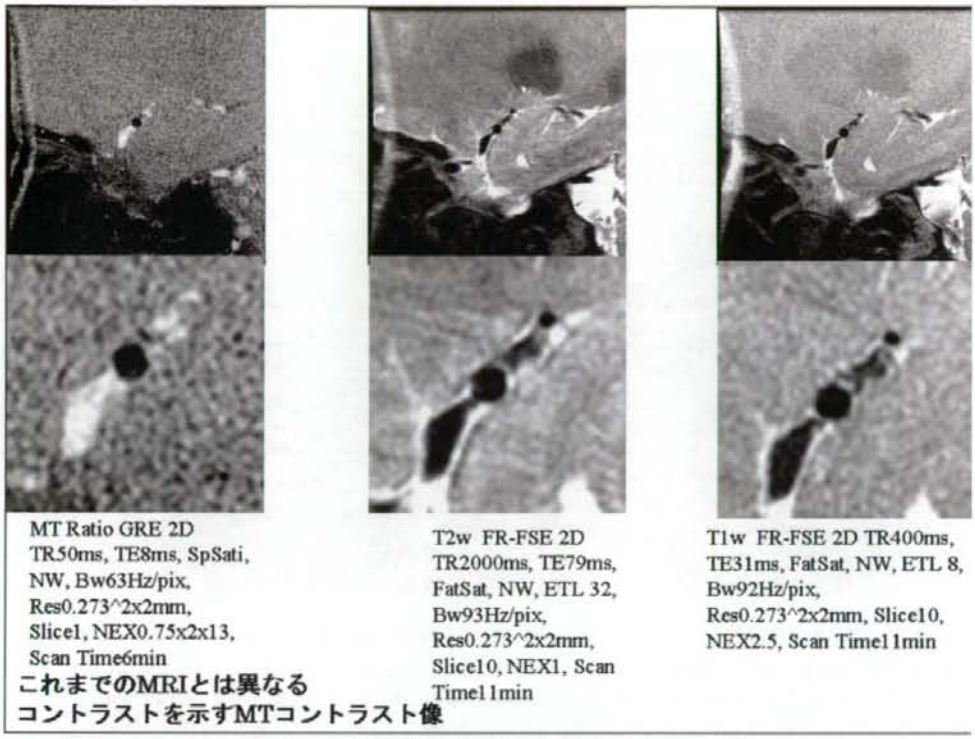

図３　頭蓋内MCA　磁化移動比像と横緩和強調像、縦緩和強調像

図４　2重反転回復法のマルチスライス化

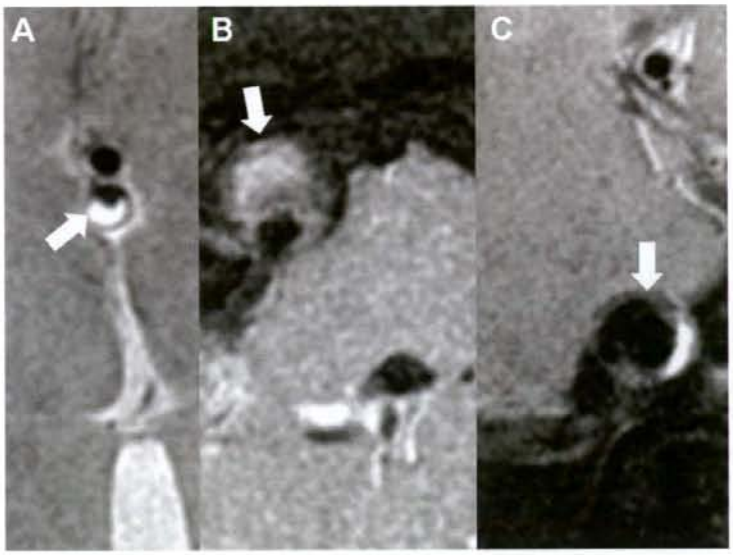

図５　脳底動脈部病態評価　**A: Arrow indicates intramural hematoma in patients with A2 dissection. B: Arrow points to thrombosed clot in dissecting aneurysm in a patient with intracranial vertebral artery dissection. C: Arrow indicates double lumen in a patient with intracranial vertebral artery dissection.** 脳底部動脈における血腫、血栓、解離を描出することが可能となった。

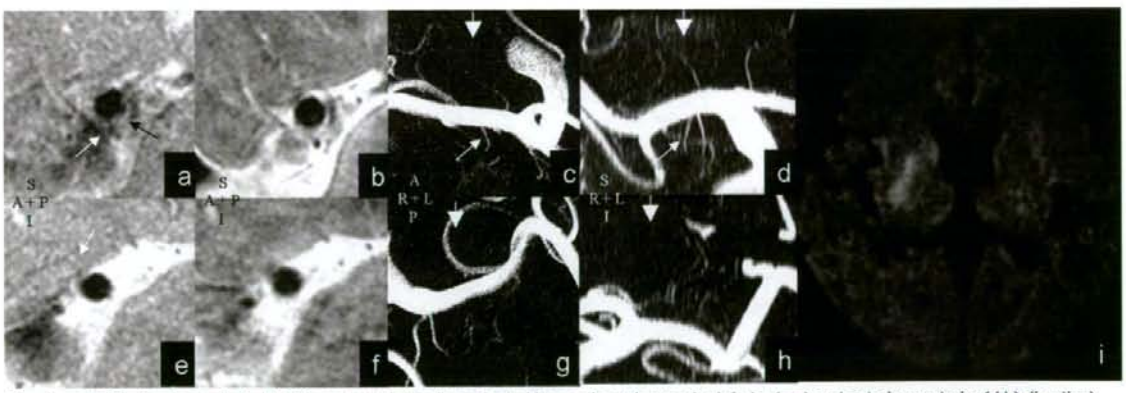

Fig. 1 sagital T_1w(a,e), T_2w(b,f), MRA (maximum intensity projected image through superior-inferior (c,g) and anterior-posterior (d,h) direction) images of possible MCA-M1 BAD patient at affected right side (a-d) and normal left side (e-h) and DWI(i). Black arrows show possible plaque, white arrows show perforators and white arrow heads show slice locations of T_1w and T_2w images.

図６　中大脳動脈病態評価　左列より縦緩和強調像、横緩和強調像、アンギオグラフィ（**S-I**方向）、アンギオグラフィ（**A-P**方向）、拡散強調像を示し、上段は患側、下段は健側を示す。**BAD**患者において患側　**Perforator**起始部における梗塞を疑わせる所見が画像より確認できた。

D. 考察

病状がよく動きの少ない患者においては良好な画像が得られ、高分解能、マルチコントラスト画像群による多角的な評価が可能であった。患者10名中2名は動きによるアーチファクトのため評価が困難であった。病状によっては撮像中の静止が困難であり、より高速、高感度の撮像法が望まれる。また疑われる病態によってはマルチコントラスト評価のうち、いくつかを省略して、時間を短縮するなどより詳細な検討が今後望まれる。またこの結果をさらに応用し、FDG-PET画像との重ね合わせや、情報の有機的な評価による読影指標の確立につなげていくべきである。

E. 結論

磁場強度３Tの臨床用MRI装置において、4チャンネルPhasedArrayコイルをプラーク描出に応用し、マルチコントラスト撮像シーケンスを最適化した。得られた結果を患者で評価し、十分なコントラストと解像度が得られることを確認した。

F. 研究発表

（発表誌名巻号・頁・発行年等も記入）

1.論文発表

なし

2.学会発表

Konosuke Furuta, Masatoshi Koga, Kazunori Toyoda, Toshiyuki Uehara, Hideki Matsuoka, Hideki Okatsu, Akihide Yamamoto, Hiroshi Sato, Takuya Hayashi, Hidehiro Iida, Kazuo Minematsu, Subtle Plaque Formation of an Intracranial Artery in Progressing Stroke Revealed by High Resolution 3-Tesla MRI, American Stroke Association 2008

Hideki Okatsu, Masatoshi Koga, Hideki Matsuoka, Konosuke Furuta, Kazunori Toyoda, Toshiyuki Uehara, Akihide Yamamoto, Hiroshi Sato, Takuya Hayashi, Hidehiro Iida, Hiroaki Naritomi, Kazuo Minematsu, High Resolution Imaging of Intracranial Arterial Dissection by 3-Tesla MRI International Stroke Conference 2008

大勝秀樹、松岡秀樹、古賀政利、豊田一則、古田興之介、上原敏志、山本明秀、佐藤博司、林　拓也、飯田秀博、成冨博章、峰松一夫　3T-MRIによる頭蓋内脳動脈解離の診断　日本脳循環代謝学会　2008

古田興之介，古賀政利，豊田一則，佐藤博司，松岡秀樹、上原敏志，山本明秀，林拓也，飯田秀博，峰松一夫　3Tesla-MRIによる頭蓋内主幹脳動脈のプラーク評価　日本神経学会総会 2008

G. 知的所有権の出願・登録状況

（予定を含む。）

1.特許取得

なし

2.実用新案登録

なし

3.その他

なし

III. 研究成果の刊行に関する一覧表

書籍

著者氏名	論文タイトル名	書籍全体の編集者名	書　籍　名	出版社名	出版地	出版年	ページ
石田良雄、木曽啓祐	4心疾患の分子イメージング 1）心筋エネルギー代謝	佐治英郎 田畑泰彦	遺伝子医学MOOK9「ますます広がる分子イメージング技術」生物医学研究から創薬、先端医療までを支える分子イメージング技術・DDSとの技術融合	株式会社メディカルドゥ	大阪	2008年	p. 225-231

雑誌

発表者氏名	論文タイトル名	発表誌名	巻号	ページ	出版年
Iida H, Eberl S, Kim KM, Tamura Y, Ono Y, Nakazawa M, Sohlberg A, Zeniya T, Hayashi T, Watabe H.	Absolute quantitation of myocardial blood flow with ^{201}Tl and dynamic SPECT in canine: optimisation and validation of kinetic modelling.	Eur J Nucl Med Mol Imaging	35	896-905	2008
Kudomi N, Slimani L, Jarvisalo M, Kiss J, Lautamaki R, Naum G, Savunen T, Knuuti J, Iida H, Nuutila P, Iozzo P.	Non-invasive estimation of hepatic blood perfusion from $H_2{}^{15}O$ PET images using tissue-derived arterial and portal input functions.	Eur J Nucl Med Mol Imaging	35	1899-911	2008
Sato H, Enmi J, Teramoto N, Hayashi T, Yamamoto A, Tsuji T, Naito H, Iida H.	Comparison of Gd-DTPA-induced signal enhancements in rat brain C6 glioma among different pulse sequences in 3-Tesla magnetic resonance imaging.	Acta Radiol.	22	667-75,	2008

Sohlberg A, Watabe H, Iida H.	Acceleration of Monte Carlo-based scatter compensation for cardiac SPECT.	Phys Med Biol.	53	277-85	2008
Yamamoto A, Sato H, Enmi J, Ishida K, Ose T, Kimura A, Fujiwara H, Watabe H, Hayashi T, Iida H.	Use of clinical MRI scanner for pre-clinical research on rats.	Radiological Physics and Technology.	2(1)	13-21	2008
Yokoyama I, Inoue Y, Kinoshita T, Itoh H, Kanno I, Iida H.	Heart and Brain Circulation and CO_2 in Healthy Men.	Acta Physiol (Oxf)	193	303-8	2008
越野 一博, 寺本 昇, 合瀬 恭幸, 福田 肇, 樋掛 正明, 渡部 浩司, 飯田 秀博	心筋PET検査の有用性	臨床画像	24	157-64	2008
飯田 秀博.	特集/分子イメージング時代の画像解析・データ解析の新しい視点-特集のねらい-New Image Processing Technologies for Clinical and Pre-clinical Molecurlar Imaging	Med Imag Tech.	26	1-2	2008
林 拓也, 武信 洋平, 久冨信之, 渡部浩司, 寺本 昇, 佐藤 博司, 越野 一博, 岩西 雄大, 永沼雅基, 森脇 博, 横田 千晶, 成富 博章, 峰松一夫, 飯田 秀博	神経画像法を用いた虚血性脳疾患の前臨床・臨床試験と病態把握.	循環器病研究の進歩	48	79-86	2008

Kudomi N., Hayashi T., Watabe H., Teramoto N., Piao R., Ose T., Koshino K., Ohta Y., Iida H.	A physiologic model for recirculation water correction in $CMRO_2$ assessment with $^{15}O_2$ inhalation PET	JCBFM	29	355-364	2008
Shidahara M., Watabe H., Kim K. M., Kudomi N., Ito H., Iida H.	Optimal scan time of oxygen-15-labeled gas inhalation autoradiographic method for measurement of cerebral oxygen extraction fraction and cerebral oxygen metabolic rate	Ann Nucl Med	22	667-675	2008
銭谷勉、渡部浩司、工藤博幸、飯田秀博	高解像度定量ピンホールSPECTイメージング—小動物から臨床へ—	映像情報メディカル	40巻、13号	1210-1215	2008
T. Zeniya, H. Watabe, H. Kudo, Y. Hirano, K. Minato, H. Iida	Clinical usability of a compact high resolution detector for high resolution and quantitative SPECT imaging in a selected small ROI	2008 IEEE Nuclear Science Symposium Conference Record		4257-4259	2008
T. Zeniya, H. Watabe, H. Kudo, Y. Hirano, K. Minato, H. Iida	Combination of a high resolution detector with small FOV and a low resolution detector with large FOV for high resolution and quantitative SPECT	2008 IEEE Nuclear Science Symposium Conference Record		5229-5231	2008
Iwanaga Y, Kihara Y, Niizuma S, Noguchi T, Nonogi H, Kita T, Goto Y.	BNP in overweight and obese patients with heart failure : an analysis based on the BNP-LV diastolic wall stress relationship	J Card Fail.	13(8)	663-7	2007

Otsuka Y, Noguchi T, Goto Y, Nonogi H, Yamada N.	Hyperintensity on T2-weighted magnetic resonance imaging in Takotsubo cardiomyopathy	Int J Cardiol.	130(1)	113-6	2008
Tomohito Hishikawa, Koji Iihara, Hatsue Ishibashi-Ueda, Kazuyuki Nagatsuka, Naoaki Yamada, Susumu Miyamoto.	Virtual Histology - intra vascular ultrasound in assessment of carotid plaques: ex-vivo study.	Nerosurgery 2009 in press			
Yamaoka M, Noda T, Nagasawa H, Naganuma M, Otsubo R, Okamura H, Ishibashi-Ueda H, Kamakura S.	Asystole caused by vegetation and abscess of right ventricle attached to a tip of pacemaker lead.	Pacing Clin Electrophysiol	31(8):	1083-4	2008
Nishi I, Noguchi T, Furuichi S, Iwanaga Y, Kim J, Ohya H, Aihara N, Takaki H, Goto Y.	Are cardiac events during exercise therapy for heart failure predictable from the baseline variables?	Circ J.	71(7)	1035-9	2007
Furuichi S, Itoh A, Ishibashi-Ueda H, Noguchi T, Miyawaki M, Nomura K, Arita Y, Otsuka M, Shindo T.	Ultrasound attenuated coronary plaque as a risk factor for slow flow or no-reflow during percutaneous coronary intervention: a case report	J Cardiol.	49(4)	193-7	2007
Tsuda E, Matsuo M, Naito H, Noguchi T, Nonogi H, Echigo S.	Clinical features in adults with coronary arterial lesions caused by presumed Kawasaki disease	Cardiol Young	17(1)	84-89	2007

T. Kawasaki, S. Koga, N. Koga, T. Noguchi, H. Tanaka, H. Koga, T. Serikawa, Y. Orita, T. Fukuyama.	Characterization of Hyperintense Plaque with Non-contrast T1-weighted Cardiovascular Magnetic Resonance Coronary Plaque Imaging : Comparison with Multislice Computed Tomography and Intravascular Ultrasound.	JACC-Imaging 2009 In press.			
石田良雄	全身疾患に合併する心血管疾患	日本医師会雑誌	137(1)	s15-s16	2008
福地一樹、石田良雄	Can 18F-Fluorodeoxyglucose Positron Tomography Imaging Provide a Noninvasive Measure of Plaque Information?	日濁医報	53(2)	52-58	2008

IV. 研究成果の刊行物・別刷

Eur J Nucl Med Mol Imaging
DOI 10.1007/s00259-007-0654-4

ORIGINAL ARTICLE

Absolute quantitation of myocardial blood flow with ^{201}Tl and dynamic SPECT in canine: optimisation and validation of kinetic modelling

Hidehiro Iida · Stefan Eberl · Kyeong-Min Kim · Yoshikazu Tamura · Yukihiko Ono · Mayumi Nakazawa · Antti Sohlberg · Tsutomu Zeniya · Takuya Hayashi · Hiroshi Watabe

Received: 18 September 2007 / Accepted: 4 November 2007

Abstract
Purpose ^{201}Tl has been extensively used for myocardial perfusion and viability assessment. Unlike ^{99m}Tc-labelled agents, such as ^{99m}Tc-sestamibi and ^{99m}Tc-tetrofosmine, the regional concentration of ^{201}Tl varies with time. This study is intended to validate a kinetic modelling approach for in vivo quantitative estimation of regional myocardial blood flow (MBF) and volume of distribution of ^{201}Tl using dynamic SPECT.
Methods Dynamic SPECT was carried out on 20 normal canines after the intravenous administration of ^{201}Tl using a commercial SPECT system. Seven animals were studied at rest, nine during adenosine infusion, and four after beta-blocker administration. Quantitative images were reconstructed with a previously validated technique, employing OS-EM with attenuation-correction, and transmission-dependent convolution subtraction scatter correction. Measured regional time–activity curves in myocardial segments were fitted to two- and three-compartment models. Regional MBF was defined as the influx rate constant (K_1) with corrections for the partial volume effect, haematocrit and limited first-pass extraction fraction, and was compared with that determined from radio-labelled microspheres experiments.
Results Regional time–activity curves responded well to pharmacological stress. Quantitative MBF values were higher with adenosine and decreased after beta-blocker compared to a resting condition. MBFs obtained with SPECT (MBF_{SPECT}) correlated well with the MBF values obtained by the radio-labelled microspheres (MBF_{MS}) ($MBF_{SPECT}=-0.067+1.042\times MBF_{MS}$, $p<0.001$). The three-compartment model provided better fit than the two-compartment model, but the difference in MBF values between the two methods was small and could be accounted for with a simple linear regression.
Conclusion Absolute quantitation of regional MBF, for a wide physiological flow range, appears to be feasible using ^{201}Tl and dynamic SPECT.

Keywords Myocardial blood flow · Dynamic SPECT · Thallium-201 · Compartment model · Quantitation

H. Iida (✉) · S. Eberl · K.-M. Kim · M. Nakazawa · A. Sohlberg · T. Zeniya · T. Hayashi · H. Watabe
Department of Investigative Radiology,
National Cardiovascular Center Research Institute,
Fujishiro-dai,
Suita City, Osaka 565-8565, Japan
e-mail: iida@ri.ncvc.go.jp

S. Eberl
PET and Nuclear Medicine Department,
Royal Prince Alfred Hospital,
Missenden Road,
Camperdown, NSW 2050, Australia

Y. Tamura
Department of Cardiology, Akita Kumiai General Hospital,
1-1-1, Nishi-bukuro, Iijima,
Akita City 011-0948, Japan

Y. Ono
Akita Research Institute of Brain,
6-10, Senshu-Kubota Machi,
Akita City 010-0874, Japan

Introduction

Myocardial perfusion imaging using Thallium-201 (^{201}Tl) is well established in routine clinical practice for detecting

exercise-induced myocardial ischaemia and/or for assessing myocardial viability in patients with coronary artery disease. The diagnosis, however, has been limited to qualitative or visual assessment of the physical extent of the defect areas rather than quantitative assessment of physiological functions. Quantitative methods would for example enable longitudinal studies when assessing therapy response and pharmacological interventions. Some groups have already investigated the feasibility of estimating quantitative parameters with dynamic SPECT in the myocardium using ^{201}Tl [1] and ^{99m}Tc-Teboroxime [1, 2], but these techniques have not yet been applied to clinical practice. This is largely attributed to the fact that quantitative reconstruction programmes are not readily available on commercial SPECT systems.

We have developed a reconstruction programme package for SPECT, which can accurately provide quantitative images of radio-labelled tracer distributions in vivo, which is a pre-requisite for absolute physiological parameter estimation. The adequacy and accuracy of these methods have been demonstrated in multiple papers for ^{99m}Tc and ^{201}Tl in cardiac studies [3–5], and for ^{99m}Tc and ^{123}I in brain studies [6]. It has also been demonstrated, in brain studies, that physiological parameters such as cerebral perfusion [6] and cerebral flow reactivity [7] obtained using our package were as accurate as those determined by PET. These findings suggest that absolute quantitation of regional myocardial perfusion might also be possible in a clinical setting using commercial SPECT cameras.

^{201}Tl is a potassium analogue, and its kinetics has been extensively investigated in previous studies [8, 9]. Due to the high first-pass extraction fraction (EF) [10] and a large distribution volume, ^{201}Tl has been considered an ideal tracer for quantitation of absolute myocardial blood flow, not only at rest but also at hyperemic conditions. As a clinical implication, quantitative assessment of MBF and coronary flow reserve is important. For instance, coronary microvascular dysfunction or impaired endothelial function in patients with coronary risk factors or patients with cardiomyopathy or with heart failure is an un-resolved important issue to answer [11]. Coronary flow reserve can also be reduced in patients with hyper-cholesterolemia without overt coronary stenosis [12]. The low energy and long half-life of ^{201}Tl have, however, seriously limited its use in nuclear cardiology.

The goal of this study was to validate our reconstruction methodology for the estimation of myocardial blood flow using ^{201}Tl and dynamic SPECT using tissue time–activity curves (TTAC) derived from myocardial regions. In addition, we aimed to find the optimal kinetic model configuration and to investigate the factors affecting the estimation of physiological parameters such as the partial volume effect (PVE), appropriate choice of input function, conversion from plasma to blood flow using haematocrit (Hct) and the limited first-pass tracer EF.

Materials and methods

Subjects

A total of 21 dogs were studied in which 8 were in a resting condition, 9 dogs during constant infusion of adenosine for increased MBF, and 4 dogs during constant infusion of beta-blocker. Of the 21 studies, 1 study was un-successful and projection data could not be retrieved from the scanner, reducing the number of resting studies to 7 and total dog studies to 20. Adenosine was infused continuously over the study duration at a rate ranging from 140 to 700 mg/kg/h to achieve a range of blood flow increases. An initial dose of beta-blockers ranging from 2 to 6 mg was given, followed by a constant infusion for the duration of the study of 2 or 4 mg/h. The study protocol was approved by the animal ethics committee at the Akita Research Institute of Brain, Akita City, Japan where all experiments were carried out.

SPECT procedures

All dogs were anaesthetised, and the catheters for dose administration and arterial blood sampling were inserted before the study. The SPECT system was a conventional dual-head gamma camera (Toshiba GCA-7200A, Tokyo, Japan) fitted with short focal length fan-beam collimators (LEHR-Fan). The transverse field-of-view (FOV) was 22 cm diameter and axial FOV was 20 cm. The dogs were carefully taped into a cradle to minimise motion during the study, and also to ensure that no truncation occurred. Heart rate and blood pressure were monitored throughout the study and recorded at regular intervals.

Before the injection of any tracer, a 15-min transmission study was carried out in which a rod source filled with approximately 740 MBq of ^{99m}Tc was placed along the focal line of one of the fan-beam collimators (see Fig. 1). The transmission study was followed by injection of 3 MBq of ^{141}Ce microspheres into the left ventricle via a catheter and blood was withdrawn from the aorta at a constant flow rate of 5 ml/min for 2 min to serve as an input function. For the pharmacological intervention studies, adenosine infusion or beta-blocker injection followed by infusion was commenced before the ^{141}Ce microsphere administration.

Dynamic SPECT was commenced with the start of the 4-min constant infusion of 110 MBq ^{201}Tl. The frame collection rates and 360° rotation times were 10×1 min (rotation time 15 s), 6×2 min (30 s), 3×4 min (60 s) and 5×5 min (60 s) for the first hour for all studies. Resting blood flow studies had an additional 18×10 min (120 s) frames collected for a total study period over 4 h. The shorter total study time for the drug infusion studies was mandated by the difficulties in keeping the dogs stable with prolonged infusions of the drugs used. A 34% energy

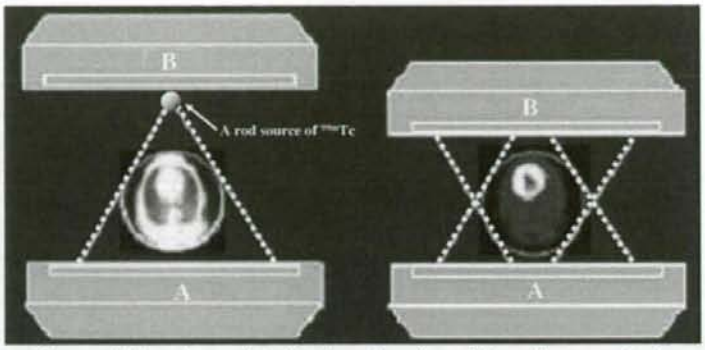

Fig. 1 Schematic diagram of data acquisition using a clinical dual-headed SPECT camera fitted with fan-beam collimators. Transmission scan was performed using a ^{99m}Tc-filled rod source placed at a focal line of one of the collimators, and only one of the detectors was used (*left*). Both detectors were used in the emission scan (*right*)

window centred on 77 keV was used for the ^{201}Tl acquisitions [4, 13].

Arterial blood samples were taken every 20 s for the first 6 min, every 60 s for 6–10 min, 120 s for 10–20 min, 300 s for 20–30 min and 600 s for 30–60 min. For the resting studies, blood samples were also taken every 20 min for 1–2 h and additional samples at 2.5, 3 and 4 h post-^{201}Tl infusion. In six studies, plasma was separated immediately after sampling by centrifugation, and plasma samples were counted in a well counter cross-calibrated with the SPECT scanner. To minimise the effects of the continued exchange of ^{201}Tl between plasma and red blood cells in the test tubes after sampling, immediate, rapid separation of plasma from whole blood was required. An averaged relationship between plasma and whole blood concentration ratio over time was obtained, and then multiplied with the whole blood curves for all studies to derive a plasma input function.

At the end of the SPECT study, the microsphere blood flow measurement was repeated with ^{51}Cr microspheres. The dogs were then killed by injection of potassium chloride (KCl) and the myocardium was dissected into samples suitable for counting in the well counter. The ^{201}Tl concentration in the tissue samples was derived from the sample weight normalised gamma counter counts. The samples were stored to allow for the decay of ^{201}Tl ($T_{1/2}$= 73 h vs $T_{1/2}$=32.5 days for ^{141}Ce and 27.8 days for ^{51}Cr) and then counted to measure the ^{141}Ce and ^{51}Cr activities. Separation between ^{141}Ce and ^{51}Cr counts was based on their respective gamma ray energies (145 keV for ^{141}Ce and 323 keV for ^{51}Cr).

SPECT data processing

Projection data were processed according to previously described procedures [5]. Briefly, the transmission data obtained by the fan-beam collimator were first re-binned into parallel projections. Transmission projections were normalised by blank projection, re-constructed to generate quantitative maps of the attenuation coefficient for ^{99m}Tc and then linearly scaled to provide attenuation correction maps for ^{201}Tl. Emission data were corrected for detector non-uniformity and also re-binned into parallel projections. The projection data were then corrected for scatter with transmission-dependent convolution subtraction (TDCS) originally proposed by Meikle et al. [14] and further optimised by our group [4, 5]. The emission projection data were re-constructed with the OS-EM reconstruction algorithm [15] using three iterations and ten subsets. The re-constructed images were cross-calibrated with the well counter system.

Data analysis

Re-constructed images were normalised by acquisition time for each frame. Multiple circular regions of interest (ROI) were drawn on the myocardium, and the TTAC of ^{201}Tl were generated for the anterior, apical, lateral, posterior and septal areas of the myocardium. The two-compartment model (one tissue compartment) and three-compartment model (two tissue compartments) shown in Fig. 2 were applied to determine two parameters (K_1 and K_2) for the two-compartment model and four parameters (K_1–K_4) for the three-compartment model by means of non-linear least squares fitting (NLLSF).

The regional MBF was considered to be related to K_1 obtained from compartment model fits. K_1 is, however, affected by the PVE, Hct and the limited first-pass EF whose effects were corrected according to Eq. 1:

$$\mathrm{MBF} = \frac{\mathrm{PVE}}{\mathrm{EF} \times (1 - \mathrm{Hct})} \times K_1 \quad (1)$$

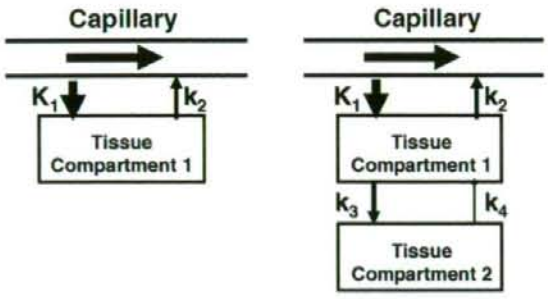

Fig. 2 Two- and three-compartment models evaluated in this study. K_1 in units of ml/min/g denotes the regional MBF for both models. Distribution volume (V_d) in units of ml/g is defined as K_1/k_2 for the two-compartment mode, and $\frac{K_1}{k_2}\left(1+\frac{k_3}{k_4}\right)$ for the three-compartment model

The physiological basis for the correction factors in Eq. 1 can be described as follows:

1. TTACs obtained from SPECT images are under-estimated due to the limited spatial resolution relative to the myocardial wall thickness and also due the myocardial contractile motion. This phenomenon is known as PVE. The PVE correction factor for each TTAC was determined from the ratio of the last SPECT frame counts to the ^{201}Tl myocardial tissue sample counts obtained from the tissue samples taken and measured with the well counter at the end of the SPECT scan.
2. The arterial input function for the compartment model studies was defined from the plasma radioactivity concentration curve, rather than the whole blood radioactivity curve. K_1 is therefore the regional "plasma" flow. Thus, for comparison with the microsphere flow measurements, which estimates the whole blood flow, K_1 was divided by (1−Hct) to obtain the flow for the total blood.
3. For a tracer with limited first-pass EF<1.0, flow (MBF) is related to K_1 by K_1=EF×MBF. The first-pass EF is flow-dependent and decreases at high flow. We have applied an empirical formulation for the first-pass EF based on the data by Weich et al. [10] (EF=0.84−0.524·$\log_{10}(K_1^*)$ where K_1^* is $K_1/(1-\text{Hct})$. The K_1 values obtained with two- and three-compartment models with/without corrections according to Eq. 1 were compared to the average of microsphere blood flow values obtained pre- and post-dynamic SPECT scan.

The distribution volume of ^{201}Tl (V_d) was defined as

$$V_d = \frac{K_1}{k_2} \text{ for the two} - \text{compartment model} \quad (2a)$$

$$V_d = \frac{K_1}{K_2}\left(1+\frac{K_3}{K_4}\right) \text{ for the three} - \text{compartment model.} \quad (2b)$$

As mentioned before, the resting studies were collected for 4 h, whilst the adenosine and beta-blocker studies were collected for approximately 1 h. To investigate whether the shorter collection time introduces systematic bias, NLLSF fits restricted to the first 1 h of the resting study data were also performed and compared with the V_d values from the full 4 h resting data set and with the estimates obtained from the beta-blocker and adenosine studies.

Akaike information criterion (AIC) and Schwarz criterion (SC) were calculated for both two-compartment and three-compartment model fits [16] to test the adequacy of the two models. All data are presented as mean±1 SD. Student's t test was employed in the comparison of the V_d values. Pearson's regression analysis was applied to compare K_1 and microsphere flow values. A probability value of <0.05 was considered statistically significant.

Results

Figure 3 shows the plasma to whole blood concentration ratios in the six dogs with rapid plasma separation and the averaged data. Equilibrium is reached after about 40 min, at which time the mean ratio was found to be 0.76. As expected, relative plasma concentration is highest early on as the tracer is injected into the plasma (and not red blood cells). ^{201}Tl is rapidly cleared from the plasma causing a rapid decline in relative plasma concentration and "undershoot" before equilibrium is established. Samples left for a prolonged period before plasma separation showed the value of approximately 0.78, which was close to the plasma to whole blood concentrations ratio at the equilibrium shown in

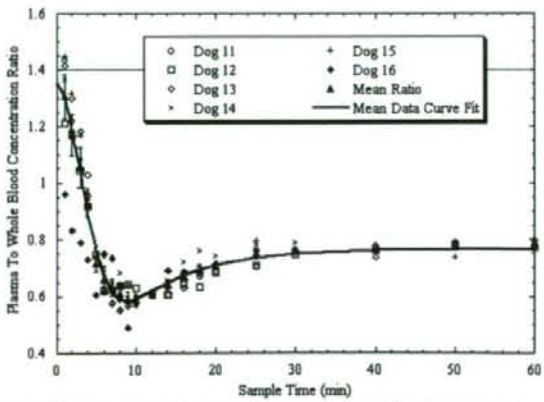

Fig. 3 Individual and mean plasma to whole blood concentration ratios over time for the six dogs with rapid plasma separation. *Error bars* indicate the standard error of the mean. *Solid line* is the curve fit to mean ratio data

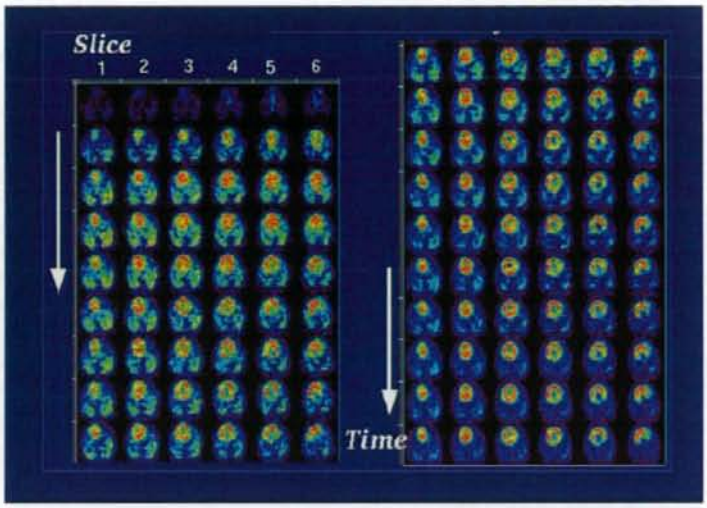

Fig. 4 A typical example of sequential SPECT images of the myocardium for six representative slices after intravenous injection of ^{201}Tl into a canine at rest

Fig. 3. The plasma to whole blood ratio curves could be approximated by the following equation:

$$R_{pl/wb} = A_0 e^{-\lambda(t+\Delta t)^2} + A_1\left(1 - e^{-\lambda_2(t+\Delta t)}\right), \quad (3)$$

which resulted in A_0=1.303±0.045, A_1=0.7649±0.0056, λ_1=0.03636±0.0039 min^{-1}, λ_2=0.1263±0.0077 min^{-1} and Δt=0.9516±0.41 min. The correlation coefficient for the fit was r=0.995.

Figure 4 shows a typical example of sequential images after the intravenous injection of ^{201}Tl for six representative slices of a dog studied at rest. It can be seen that ^{201}Tl appeared in the ventricular chambers first and then gradually accumulated homogeneously into the left myocardium. The quality of these images is reasonably good, indicating that our approach of estimating the kinetic parameters by NLLSF is feasible without excessive noise

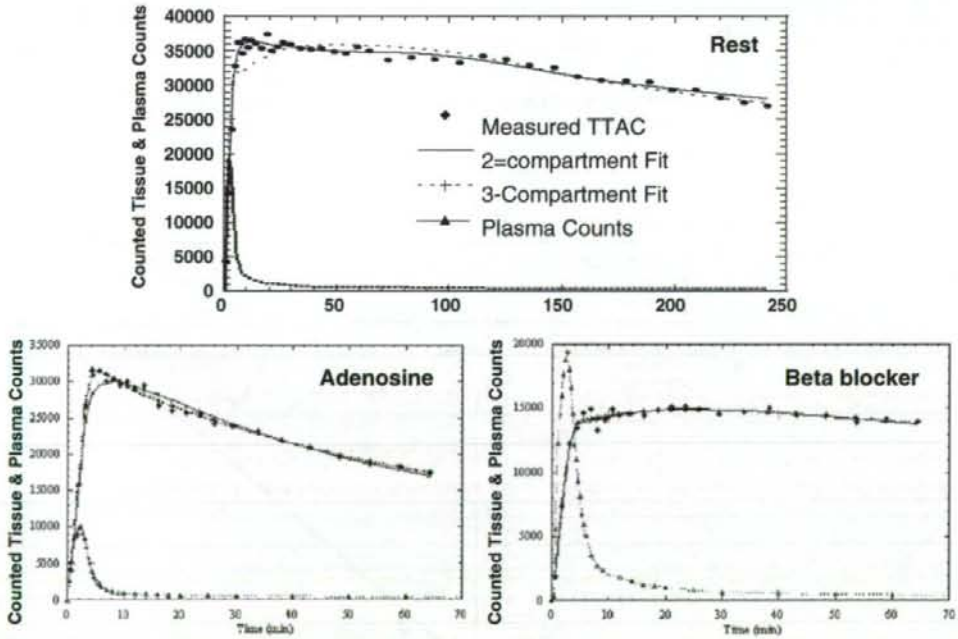

Fig. 5 TTACs and two- and three-compartment model fits for a resting, adenosine (increased MBF) and beta-blocker (reduced MBF) study. Note the different time scales for the resting study because resting studies were collected for 4 h compared to ≈1 h for the pharmacological intervention studies

amplification. Curve fits to representative TTACs for resting, beta-blocker and adenosine infusion studies are shown in Fig. 5. The height of the TTACs relative to the input function corresponded well with the pharmacological challenges. Compared to the resting studies, peaks of TTACs relative to the arterial input function were higher for adenosine and lower after beta-blocker administration. Results of kinetic fitting by the two- and three-compartment models are also plotted on this figure. Visually, the three-compartment model provided better fits than the two-compartment model to the observed TTACs, which is particularly evident for the initial scan period of the resting and adenosine studies.

Shown in Fig. 6a–e is the comparisons of K_1 obtained by NLLSF (three-compartment model fit) with the microsphere flow estimates. Values were averaged over the myocardial segments in both axes, thus each point corresponds to a single study. There was good correlation between K_1 and the microsphere flow when no corrections were applied, but K_1 significantly under-estimated the true flow (Fig. 6a). All the corrections improved the K_1 estimates (Fig. 6b–d) and the best agreement between K_1 and microsphere flow was observed when all three factors were corrected as described in Eq. 1 (Fig. 6e). Results of the regression analysis also demonstrated the highest correlation coefficient when all three correction factors were applied. Table 1 summarises the results of the Akaike information criteria (AIC) and Schwartz criteria (SC) obtained from the kinetic fitting analysis for all myocardial segments of all subjects. Both

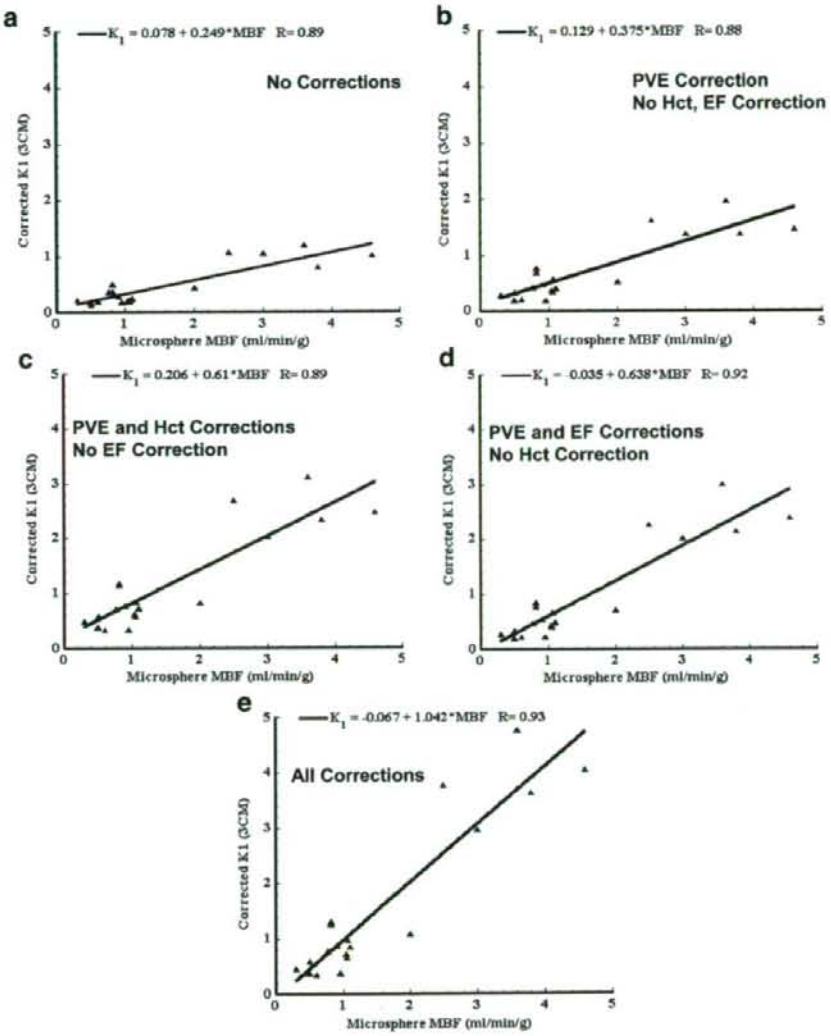

Fig. 6 Plot of K_1 derived from the three-compartment model fit against the mean of the pre- and post-dynamic SPECT microsphere blood flow measurements. **a** No correction for PVE, limited first-pass EF or conversion from plasma to blood flow has been applied. **b** Correction for PVE has been applied, but not for Hct or limited first-pass EF. **c** Corrections for PVE and Hct have been applied, but not for limited first-pass EF. **d** Corrections for PVE and limited first-pass EF have been applied, but not for Hct. **e** All corrections are applied for PVE, limited first-pass EF and Hct